

Color Tuning of Efficient Electroluminescence in the Blue and Green Regions Using Heteroleptic Iridium Complexes with 2-Phenoxyoxazole Ancillary Ligands

Helen Benjamin,[†] Jie Liang,[‡] Yu Liu,^{*,‡,§} Yun Geng,[§] Xingman Liu,[§] Dongxia Zhu,^{*,§} Andrei S. Batsanov,^{†,§} and Martin R. Bryce^{*,†,§}

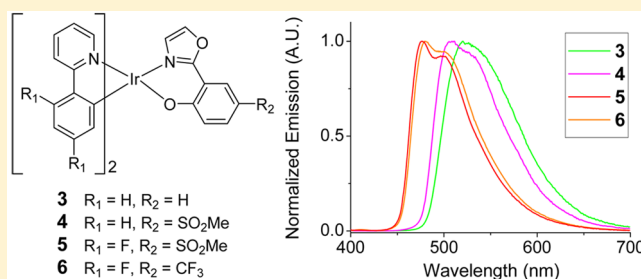
[†]Department of Chemistry, Durham University, Durham DH1 3LE, U.K.

[‡]State Key Laboratory of Supramolecular Structure and Materials, College of Chemistry, Jilin University, Changchun 130012, People's Republic of China

[§]Key Laboratory of Nanobiosensing and Nanobioanalysis at Universities of Jilin Province, Department of Chemistry, Northeast Normal University, 5268 Renmin Street, Changchun, Jilin 130024, People's Republic of China

Supporting Information

ABSTRACT: A rational molecular design strategy for tuning the emission color of phosphorescent complexes by functionalization of the bis(2-phenylpyridine)(2-(2'-oxyphenyl)-2-oxazoline/oxazole)iridium(III) framework is reported. Five new complexes (2–6) have been synthesized in good yields and characterized by cyclic voltammetry, absorption, and photoluminescence studies, by time-dependent density functional theory (TD-DFT) calculations, and by single-crystal X-ray diffraction studies for complexes 2, 4, and 6. An interesting feature of the complexes is that the HOMO is localized on the Ir d-orbitals and the phenoxyate part of the “ancillary” ligand, while the LUMO is located on the pyridyl ring of the ppy ligands. A few other complexes containing 2'-oxyphenyl-2-oxazoline/oxazole ancillary ligands have been reported previously; however, until now there has not been a systematic investigation into manipulating this unusual frontier orbital distribution to tune the emissive properties. It is shown that exchanging the phenylpyridine (ppy) ligand for 2,4-difluoro-ppy gives a blue shift of 21–22 nm (from 1 to 2 and from 4 to 5), and the introduction of electron-withdrawing substituents (SO₂Me, CF₃) onto the phenoxyate ring of the (2'-oxyphenyl)-2-oxazole ligand results in a further blue shift of 13–20 nm. Combining these functionalizations gives sky-blue emission with $\lambda_{\max}^{\text{PL}}$ 476 and 479 nm for complexes 5 and 6 in dichloromethane solution. The solution quantum yields of all the complexes are within the range Φ_{PL} 0.42–0.73. The observed lifetimes ($\tau_{\text{obs}} = 1.52$ – $3.01 \mu\text{s}$) and spectral profiles are indicative of phosphorescence from a mixture of ligand-centered and MLCT excited states. (TD-)DFT calculations are in close agreement with the observed photophysical and electrochemical properties of the complexes. Phosphorescent organic light-emitting diodes have been fabricated using complexes 2, 3, 5, and 6 as the emitter, doped in a 4,4'-bis(*N*-carbazolyl)biphenyl host, giving efficient emission in the blue-green region. Notably, complex 5 gives $\lambda_{\max}^{\text{EL}}$ 480 nm with a maximum brightness of 26150 cd m⁻².



INTRODUCTION

Luminescent transition metal complexes¹ are renowned for their applications in diverse areas such as biological probes,² responsive materials,³ water splitting, ion sensors, solar cells, phosphorescent organic light-emitting diodes (PhOLEDs), and solid-state lighting. In the context of PhOLEDs⁴ and lighting⁵ iridium(III) complexes have been at the forefront of attention since the pioneering studies of Forrest et al.,⁶ due to their outstanding combination of properties, namely, (i) synthetic versatility, (ii) good stability and color-tunability, (iii) high phosphorescence quantum efficiency, (iv) relatively short excited-state lifetimes of a few microseconds, and (v) good thin film processability. For these applications, homoleptic [Ir(C[^]N)₃] and heteroleptic iridium(III) complexes [Ir(C[^]N)₂L] are typically based on cyclometalated 2-phenyl-

pyridine (ppy) ligands where the highest occupied molecular orbital (HOMO) is primarily localized on the iridium d-orbitals and the phenyl ring, while the lowest unoccupied molecular orbital (LUMO) is predominantly located on the pyridyl ring.⁷ Emission is generally from a mixture of triplet metal-to-ligand charge-transfer (³MLCT) states and π - π^* transitions within the ligands. Electron-withdrawing groups on the phenyl ring of ppy lower the HOMO level, while electron-donating groups on the pyridyl ring increase the LUMO level.⁸ Varying the ancillary ligand in heteroleptic complexes, e.g., L = acetylacetonate,⁹ picolinate,¹⁰ bis(pyrazolyl)borate,¹¹ or pyridylazolate,¹² is also an established strategy for color tuning of emission by

Received: March 2, 2017

perturbing the MLCT interaction. In some complexes interligand energy transfer can occur from the cyclometalating ppy ligand to the ancillary ligand, e.g., with a quinoline carboxylate ancillary ligand.¹³

We recently reported that complex **1** (Figure 1), featuring a 2'-oxyphenyl-2-oxazoline ancillary ligand, showed promising

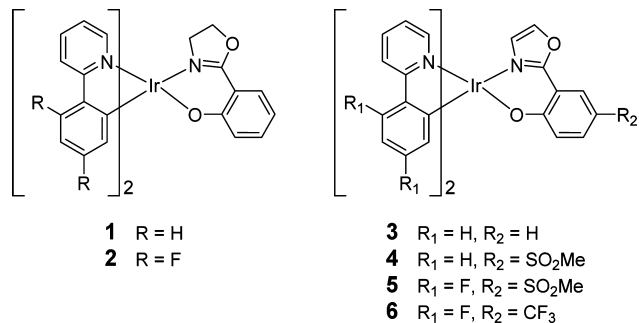


Figure 1. Chemical structures of the oxazoline (**1**, **2**) and oxazole complexes (**3–6**).

green PhOLED performance and, in particular, displayed an interesting distribution of the frontier orbitals.¹⁴ The LUMO of **1** is located on the pyridyl ring of the ppy ligands, while the HOMO is localized on the Ir d-orbitals and the phenoxy part of the “ancillary” ligand.¹⁴ A few other complexes containing 2'-oxyphenyl-2-oxazoline/oxazole ancillary ligands have been reported.¹⁵ However, there is a lack of systematic investigation into manipulating this unusual frontier orbital distribution to tune the emissive properties.

In this work we focus on the synthesis and photophysical and electrochemical properties of five new iridium(III) complexes (**2–6**), each with an oxazoline or oxazole ancillary ligand. Our targets were designed to utilize the unusual HOMO–LUMO distribution to blue shift the emission relative to complex **1**. We have successfully achieved this via simple and rational substitutions on both the phenylpyridine and the ancillary ligands. It is well documented in the literature that introducing electron-withdrawing groups, such as fluorine,¹¹ perfluoroalkyl,¹⁶ sulfonyl,^{17,18} phosphoryl,¹⁶ and cyano substituents, onto positions of HOMO localization is an effective method to blue shift the emission of the resultant iridium complex. With this in mind we introduced SO₂Me and CF₃ groups *para* to the hydroxyl on the 2-(2'-oxyphenyl)-2-oxazole ligand with the aim

of lowering the HOMO. Fluorine substituents were also introduced on the ppy ligands, even though they have little contribution to the HOMO in **1**, as it was thought they could blue shift the emission by lowering the energy of the iridium d-orbitals, a strategy that is known for ancillary ligands.¹⁰ PhOLED fabrication and efficient device performance in the blue-green region is reported for selected derivatives.

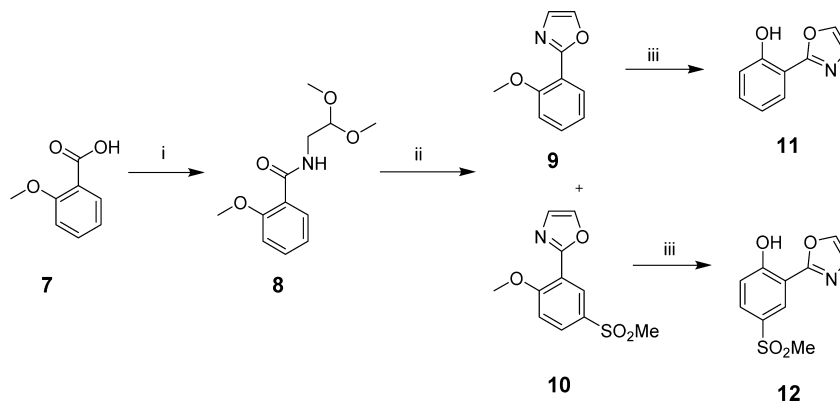
RESULTS AND DISCUSSION

Synthesis. The syntheses of the ancillary oxazole-based ligands and their derived complexes are shown in Schemes 1–3. All the complexes were characterized by NMR spectroscopy, mass spectrometry, and elemental analysis, with X-ray crystal structures of complexes **2**, **4**, and **6**. The synthesis of oxazoline ligand **21** (Scheme 3) is described in the literature.^{14,19} The oxazole-containing ligand **11** was synthesized as shown in Scheme 1, via a condensation between carboxylic acid **7** and aminoacetaldehyde diethylacetal, followed by *in situ* deprotection of the masked aldehyde **8** and oxazole formation with Eaton's reagent. Two products were isolated, the desired compound **9** and the methanesulfonyl derivative **10** (ca. 1:1 ratio). As we were interested in functionalizing the ancillary ligand, additional quantities of **10**, along with analogue **19**, were synthesized as shown in Scheme 2, as it transpired that the route in Scheme 1 was not compatible with the desired substituents on the phenyl ring. The new route (Scheme 2) involved a condensation reaction between carboxylic acids **13** and **14** and aminoacetaldehyde diethylacetal to give **15** and **16**. The next step was a deprotection of the masked aldehyde with HCl to give **17** and **18**, followed by a cyclization with Burgess' reagent under microwave conditions,²⁰ to give ligand precursors **10** and **19**. The final step in both schemes was demethylation of **9**, **10**, and **19**, which was achieved using either BBr₃ or pyridine-HCl, to afford the phenol derivatives **11**, **12**, and **20**, respectively.

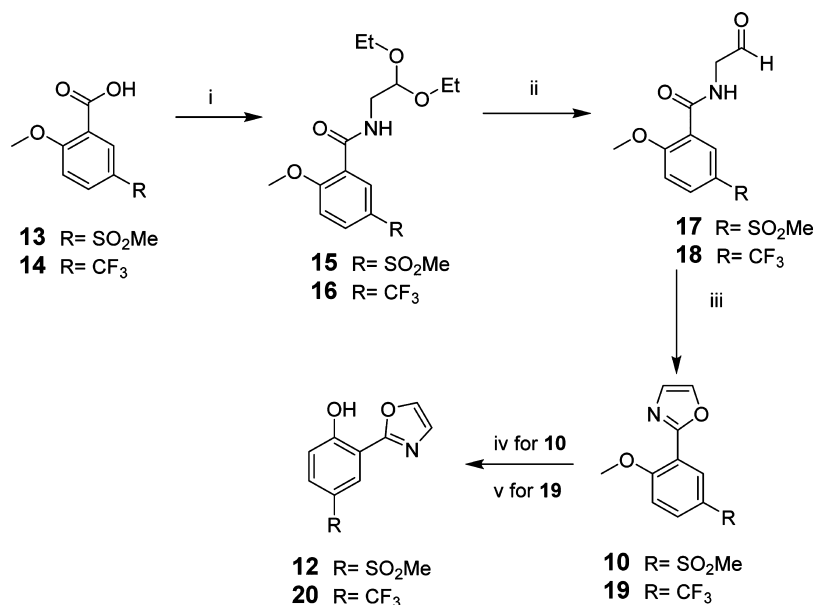
The new heteroleptic complexes **2–6** were then synthesized using standard conditions²¹ (Scheme 3).

The intermediate μ -dichloro-bridged dimer [Ir(L)₂Cl]₂ was reacted *in situ* with the appropriate ancillary ligand **11**, **12**, **20**, or **21** in the presence of Na₂CO₃. The complexes **2–6** were obtained as yellow powders in 57–87% yields. The NMR spectra of **5** and **6** were obtained in acetone-*d*₆. This was because upon storage of the solutions of **5** and **6** in CDCl₃ under ambient conditions (laboratory light at 20 °C), partial re-

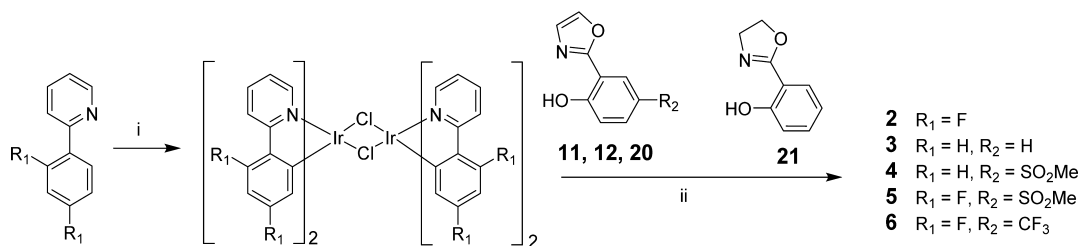
Scheme 1. Synthesis of Ancillary Ligands **11** and **12**^a



^aReagents and conditions: (i) aminoacetaldehyde diethylacetal, 160 °C, (ii) MeSO₃H/P₄O₁₀, 180 °C, (iii) BBr₃, 0 °C, DCM.

Scheme 2. Synthesis of Ancillary Ligands 12 and 20^a

^aReagents and conditions: (i) (1) SOCl₂, reflux, (2) aminoacetaldehyde diethylacetal, NEt₃, DCM, RT, (ii) catalytic HCl, acetone/water, reflux, (iii) Burgess' reagent, THF, microwaves, 70 °C, (iv) BBr₃, 0 °C, DCM, (v) pyridine-HCl, 160 °C.

Scheme 3. Synthesis of Complexes 2–6^a

^aReagents and conditions: (i) IrCl₃·3H₂O, 2-ethoxyethanol, 130 °C, (ii) ancillary ligand **11**, **12**, **20**, or **21**, Na₂CO₃, 2-ethoxyethanol, 130 °C.

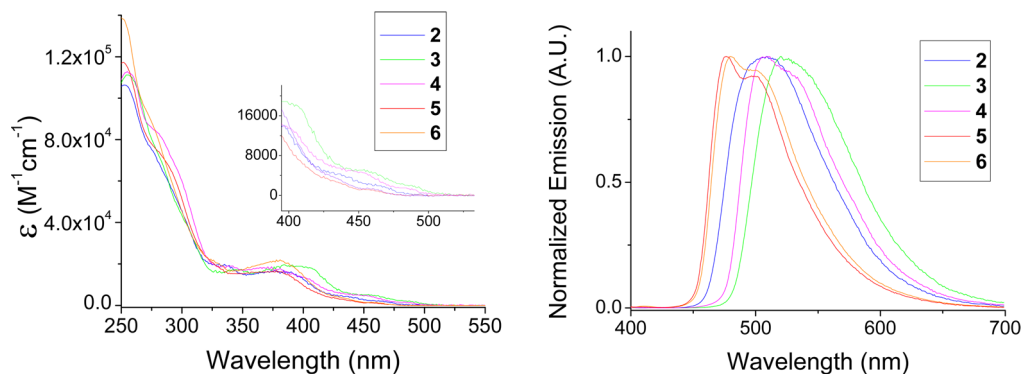


Figure 2. Absorption spectra of complexes 2–6 in DCM [$<10^{-5}$ M]. Emission spectra of complexes 2–6 in degassed DCM [$<10^{-5}$ M], $\lambda_{\text{ex}} = 355$ nm.

formation of the dichloro-bridged dimer was observed. This is ascribed to the presence of traces of acid, as noted by Baranoff et al. for previous complexes.²²

Thermal, Photophysical, and Electrochemical Properties. The thermal stabilities of the iridium complexes were evaluated using thermogravimetric analysis (TGA) under a nitrogen atmosphere. The 5% weight loss temperatures (T_d) are above 300 °C for all complexes, suggesting the complexes should be thermally stable under device operation (Table S2).

The absorption and emission spectra of complexes 2–6 in dichloromethane solutions are shown in Figure 2, and the data for 1–6 are listed in Table 1. The strong bands between 250 and 320 nm are assigned to π – π^* transitions on the ligands based on literature precedents.²³ Absorption bands in the range 350–460 nm with lower extinction coefficients are assigned to the ¹MLCT/³MLCT bands following literature precedents¹⁸ and the calculations of Hay.²⁴ Emission from the complexes is

Table 1. Photophysical Data for Iridium Complexes 1–6

complex	$\lambda_{\max}^{\text{abs}} (\epsilon)/\text{nm} (\times 10^3 \text{ M}^{-1} \text{ cm}^{-1})^a$	$\lambda_{\max}^{\text{em}}/\text{nm}^b$	PLQY/ $\Phi_{\text{PL}}^{a,c}$	$\tau_{\text{p}}/\mu\text{s}^{a,d}$	$k_{\text{r}}/10^5 \text{ s}^{-1}$	$k_{\text{nr}}/10^5 \text{ s}^{-1}$	$E^{\text{ox}}_{1/2}/\text{V}^e$	HOMO/ eV^f	T_1/eV^h
1 ^g	249, 340 (sh), 377 (sh), 443 (sh)	527	0.55	0.34	1.61	1.32	0.08	−4.88	2.51
2	252 (104.8), 275 (sh, 74.2), 334 (18.7), 374 (16.0), 390 (14.7), 438 (3.9), 464 (1.8)	506	0.65	1.52	4.28	2.30	0.37	−5.17	2.49
3	255 (119.3), 280 (sh, 79.3), 303 (sh, 43.3), 386 (20.8), 402 (18.5), 456 (5.2), 488 (2.0)	521	0.45	1.71	2.63	3.22	0.18	−4.98	2.57
4	253 (111.0), 279 (83.2), 297 (64.1), 339 (18.9), 365 (18.3), 380 (17.3), 401 (13.4), 451 (4.5), 483 (1.2)	508	0.42	1.80	2.33	3.22	0.30	−5.10	2.56
5	251 (118.6), 291 (65.5), 325 (20.6), 379 (16.2), 429 (3.5), 457 (1.4)	476, 501	0.73	3.01	2.43	0.90	0.76	−5.56	2.71
6	248 (140.3), 275 (89.9), 329 (20.3), 382 (20.7), 439 (2.6), 458 (1.2)	479, 502	0.69	2.95	2.34	1.05	0.72	−5.52	2.69

^aData obtained in dichloromethane solution at 20 °C. ^bData obtained in degassed dichloromethane solution with $\lambda_{\text{ex}} = 380 \text{ nm}$. ^cMeasured in degassed DCM relative to quinine sulfate, $\Phi_{\text{PL}} = 0.546$ in 0.5 M H_2SO_4 at 20 °C; estimated error $\pm 5\%$. ^dEstimated error $\pm 5\%$. ^eAll values are reported vs $\text{Fc}/\text{Fc}^+ = 0.00 \text{ V}$. Measured in DCM (0.1 M $^n\text{Bu}_4\text{NPF}_6$) at 298 K. ^fObtained from the electrochemical oxidation potential. ^gValues for complex 1 taken from ref 12. ^hEstimated from the onset wavelengths of the 77 K emission spectra measured in THF solution with $\lambda_{\text{ex}} = 365 \text{ nm}$ (Figure S38).

in the green/blue-green region, and the following trends are observed.

(i) Exchanging the oxazoline of the parent complex 1 for an oxazole (complex 3) results in a small blue shift of 6 nm. This could be due to the increased electron-withdrawing capability of the oxazole fragment, compared to the oxazoline, as a result of the extended conjugation.

(ii) Exchanging the ppy ligand for 2,4-difluorophenylpyridine gives a blue shift of 21–22 nm (from 1 to 2 and from 4 to 5), although computational data (see below) suggest the HOMO is localized on the phenoxylate of the ancillary ligand, not the phenyl of ppy. This change of emission color can be explained by the presence of two fluorines that could still influence the energy levels of the iridium d-orbitals, which are heavily involved in the excited state.

(iii) The introduction of electron-withdrawing moieties (SO_2Me , CF_3) onto the phenoxylate ring of the ancillary ligand results in a further blue shift of 13–20 nm. This was expected, as the HOMO in the complexes is localized on that ring (see below).

(iv) The emission profiles of the complexes 2–4 are similar to that of the parent complex 1¹⁴ and are broad and largely featureless, indicating a strong MLCT contribution to the emission. However, for complexes 5 and 6 stronger vibronic features are observed as the emission is shifted further toward the blue, suggesting an increase in the LC contribution to the emission.^{23,24}

The photoluminescence quantum yields (PLQYs), lifetimes (τ_{obs}), and calculated radiative and nonradiative decay rates (k_{r} and k_{nr}) are stated in Table 1. QYs are in the range Φ_{PL} 0.42–0.73. The observed lifetimes ($\tau_{\text{obs}} = 1.52$ – $3.01 \mu\text{s}$) are indicative of phosphorescence from a mixture of ligand-centered (LC) and MLCT excited states.^{6b,25}

Electrochemistry. The electrochemical behavior of the complexes was investigated using cyclic voltammetry (CV) in a $^n\text{Bu}_4\text{NPF}_6$ dichloromethane solution. All the complexes show an electrochemically quasi/irreversible oxidation at 0.08–0.76 V vs Fc/Fc^+ , assigned to the Ir(III)/Ir(IV) couple (Table 1, Figure 3). Exchanging the ppy ligand for dfppy (1 to 2 and 4 to 5) results in a large increase in the oxidation potential, of 0.29–0.46 V, indicating the fluorine substituents are efficient at lowering the HOMO. Introducing electron-withdrawing groups on the phenoxylate ring also increases the oxidation potential (by 0.12 V for SO_2Me ; compare 3 and 4); this is consistent with the HOMO of 4 localized primarily on the phenoxylate

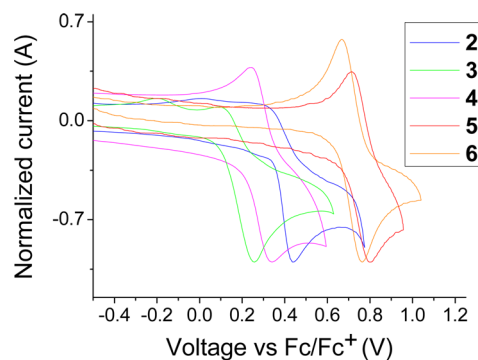


Figure 3. Cyclic voltammograms of complexes 2–6 measured in DCM (0.1 M $^n\text{Bu}_4\text{NPF}_6$) at 298 K.

ring of the ancillary ligand (see below), and introducing an electron-withdrawing group, such as a sulfone, should lower the HOMO level. Upon replacing the oxazoline fragment with an oxazole (1 to 3), the oxidation potential increases by 0.1 V. As the HOMO for 1 is localized on the iridium d-orbitals and across the phenoxylate ring, it is possible that switching from an oxazoline to an oxazole lowers the HOMO energy due to the increased electron-withdrawing ability of the oxazole compared to the oxazoline. If the LUMO energies are assumed to be very similar in these complexes, the relative HOMO energies from their CV data are consistent with the λ_{\max} values obtained from the emission spectra (Table 1). No reduction features were observed within the solvent window (scanning to -1.5 V vs Fc/Fc^+).

X-ray Crystallography. Single-crystal structures were obtained for 2, 4, and 6. In each case the Ir atom has a distorted octahedral coordination (Figure 4). The 2-(2'-oxyphenyl)-2-oxazoline/oxazole ligand is chelating the metal via its oxy and N atoms. In 2 the oxazoline ring is planar, as in the noncoordinated molecule 21 in the crystal.²⁶ The twist between the oxazoline and benzene rings in 2 is 8.1° , whereas in 21 it is practically nil; planarity of 21 is stabilized by an intramolecular O–H \cdots N bond. Nevertheless, the inter-ring bond C(2)–C(3) is shorter in 2 than in 21, 1.442(6) vs 1.462(1) Å. The oxyphenyloxazole ligand in 4 and 6 is more planar and shows a stronger π -delocalization in the chelate ring (Table 2). The C,N-chelating ppy ligands also show small but significant twists between the two aromatic systems. The Ir–C(11) bond, *trans* to the Ir–O(1), is shorter than the Ir–C(22), which is *trans* to the oxazole/oxazoline N(1), as

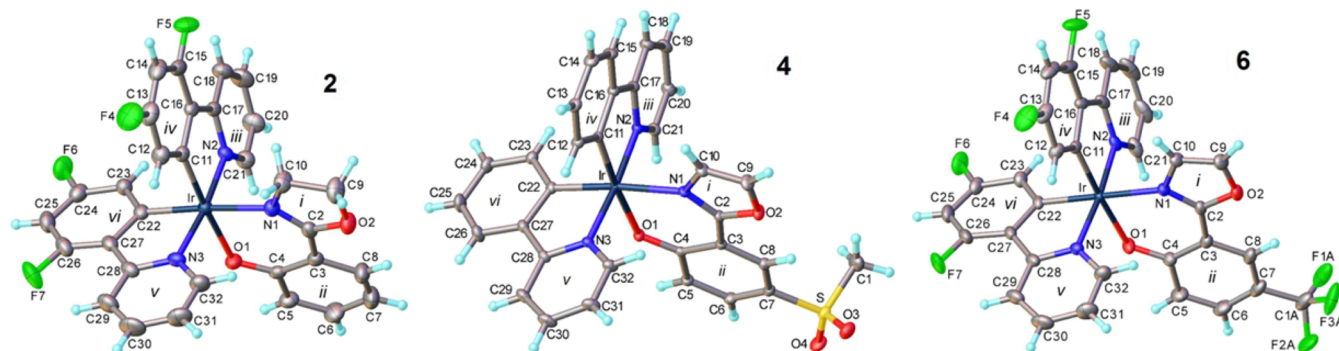


Figure 4. X-ray molecular structures of complexes **2**, **4**, and **6**. The DCM (**2**), THF (**4**), and DCM/chloroform (**6**) molecules of crystallization and the disorder of the CF₃ group in **6** are not shown. Thermal ellipsoids are drawn at the 30% (**2**) or 50% (**4**, **6**) probability level.

Table 2. Selected Bond Distances (Å) and Interplanar Angles (deg) between Mean Ring Planes

	2	4	6^a	21
Ir–O(1)	2.134(3)	2.1452(8)	2.135(2)	
Ir–N(1)	2.119(3)	2.137(1)	2.126(2)	
Ir–N(2)	2.030(3)	2.035(1)	2.031(2)	
Ir–N(3)	2.040(4)	2.042(1)	2.041(2)	
Ir–C(11)	1.979(4)	1.989(1)	1.986(2)	
Ir–C(22)	2.001(4)	2.000(1)	2.001(2)	
N(1)–C(2)	1.292(6)	1.3116(15)	1.310(3)	1.283(1)
C(2)–C(3)	1.442(6)	1.4477(16)	1.443(3)	1.462(1)
C(3)–C(4)	1.415(6)	1.4333(16)	1.428(3)	1.410(1)
O(1)–C(4)	1.293(5)	1.2890(14)	1.295(3)	1.354(1)
C(2)–O(2)	1.351(5)	1.3544(14)	1.356(2)	1.348(1)
<i>i/ii^b</i>	8.1	4.3	2.9, 3.5	0
<i>iii/iv</i>	6.2	6.8	5.9, 2.5	
<i>v/vi</i>	4.5	3.1	13.7, 9.1	

^aBond distances averaged between two independent molecules. ^bRing notation is shown in Figure 4.

expected from the *trans*-effect. The nitrogen atoms of these ligands are *trans* to each other; interestingly, in all three

complexes the Ir–N(2) bond is slightly shorter than Ir–N(3); that is, the Ir–N and Ir–C bonds in a chelate ring strengthen simultaneously.

The crystal packing of **2** shows intermolecular stacking between rigorously parallel rings *iii* and *v* and their respective inversion equivalents, the interplanar separations being *iii/iii'* 3.57 and *v/v'* 3.60 Å. This may result in a continuous chain of π – π interactions. In **6** there is also a continuous chain through intermolecular stacking of moieties *iii* and *iv*, which are only approximately parallel (interplanar angle 11.4°, average separation 3.44 Å). The molecules of **4** form no such chain but a dimer through a tight π – π contact between inversion-related moieties *v* at 3.36 Å interplanar separation and 3.69 Å distance between ring centroids, which amounts to a 1.53 Å parallel slip of the rings along the N(3)⋯C(30) direction.

Theoretical Calculations. Electronic structure calculations were performed on complexes **2**, **4**, and **6** to elucidate the nature of the transitions involved in the excitation spectra. The full geometries were optimized at the B3LYP/LANL2DZ:6-31G* level and are denoted **2'**, **4'**, and **6'** to distinguish them from experimental data. To assist in assigning the nature of the excited states involved in the experimental absorption spectra, the singlet excited states were obtained based on TD-DFT

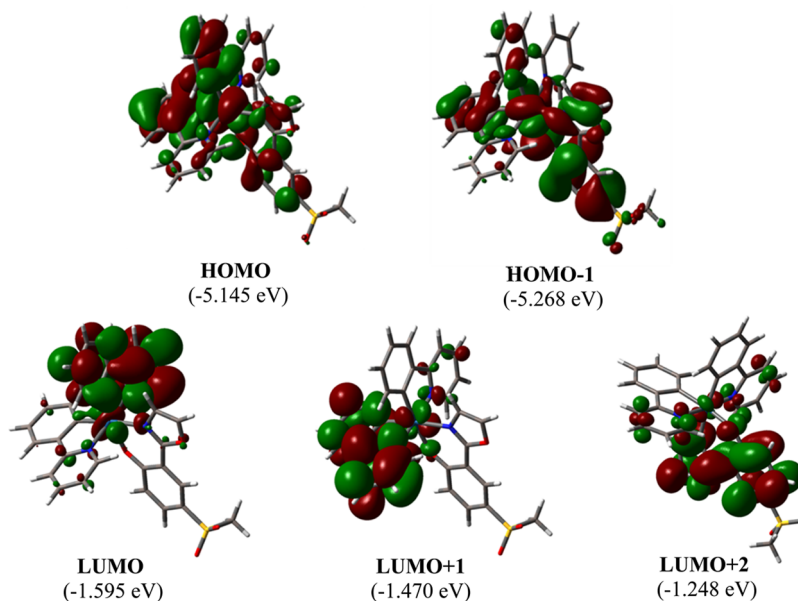


Figure 5. Contour plots of the HOMOs and LUMOs of complex **4'**.

calculations. The frontier molecular orbitals of 2', 4', and 6' are shown in Figures S1, 5, and S2, respectively, while the transition character, orbital distributions, and the simulated UV–vis absorption spectra of the complexes are summarized in Table 3. The computed orbital energies and energy gaps for 2',

Table 3. TD-DFT Calculation Results for Complexes 2', 4', and 6'

complex	transition energy ^a	participating MO	transition character ^b	energy gap/eV
2'	452.3 nm	HOMO → LUMO (96.8%)	L _C L _A CT + ML _A CT	3.35
	439.3 nm	HOMO → LUMO+1 (98.2%)	L _C L _B CT + ML _B CT + L _C L _A CT	
	376.0 nm	HOMO → LUMO+2 (93.2%)	L _C L _A CT + L _C L _B CT + ML _A CT + ML _B CT	
4'	441.4 nm	HOMO → LUMO (94.9%)	L _C L _B CT + ML _B CT + L _A L _B CT	3.55
	409.9 nm	HOMO-1 → LUMO (89.4%)	L _C L _B CT + ML _B CT	
	382.1 nm	HOMO → LUMO+2 (97.2%)	L _B L _C CT + ML _C CT + L _A L _C CT	
6'	421.07 nm	HOMO → LUMO (81.6%)	L _C L _B CT + ML _B CT	3.62
	404.25 nm	HOMO-1 → LUMO (15.3%)	L _C L _B CT + ML _B CT + L _A L _B CT	
		HOMO-1 → LUMO (75.2%)	L _C L _B CT + ML _B CT + L _A L _B CT	
	355.87 nm	HOMO → LUMO+2 (93.2%)	L _C L _B CT + ML _B CT + ML _C CT + L _B L _C CT	

^aExcitation energies calculated for the excited states. ^bLigand notation: A, B = 2-(2,4-difluorophenyl)pyridyl/2-phenylpyridyl; C = 2-(2'-oxyphenyl)-2-oxazoline/4-(methylsulfonyl)-2-(oxazol-2-yl)phenol.

4', and 6' show good agreement with the observed oxidation potentials and trends in photoluminescence measurements (Table 1). All three complexes display similar frontier orbital distributions, with the LUMOs localized mostly on the phenylpyridine-based ligands, while the HOMOs are spread across the iridium atom and the phenoxy ring of the ancillary ligand. It is noted that the HOMO of 4' also has a significant contribution from the phenyl rings of the ppy ligands.

Electrophosphorescent Device Properties. PhOLED devices of complexes 2, 3, 5, and 6 were fabricated in the following configuration: ITO/NPB (40 nm)/4,4'-bis(*N*-carbazolyl)biphenyl (CBP):Ir complex (8%) (30 nm)/TPBi (25 nm)/LiF/Al. All the devices were fabricated by thermal evaporation onto a cleaned glass substrate precoated with conductive transparent indium tin oxide (ITO), where 4,4'-bis(*N*-(1-naphthyl)-*N*-phenylamino)biphenyl (NPB) served as a hole-transporting layer and 1,3,5-tris(*N*-phenylbenzimidazol-2-yl)benzene (TPBi) as an electron-transporting layer and CBP (4,4'-bis(*N*-carbazolyl)-1,1'-biphenyl) is the host. The device structure and the corresponding energy level diagram of the respective active layers are shown in Figure 6a. Complex 4 could not be sublimed, and so devices were not fabricated. The normalized electroluminescence (EL) spectra of the devices at 1000 cd m⁻² (Figure 6b) are consistent with the photoluminescence (PL) spectra. The EL spectrum of each device did not change substantially in the whole range of driving voltages, and no host emission was observed in the EL spectra,

indicating good exciton confinement on the emissive molecules. Devices 2 and 3 showed the brightest emission in the greenish-blue ($\lambda_{\max}^{\text{EL}}$ 496 nm) and green ($\lambda_{\max}^{\text{EL}}$ 524 nm) regions, respectively. This result indicates that introducing electron-withdrawing groups such as fluorine onto the cyclometalated (C[^]N) ligand indeed leads to the larger band gap and the blue-shifted emission. Furthermore, complexes 5 and 6, which have the same C[^]N ligand as 2, exhibited sky-blue emission ($\lambda_{\max}^{\text{EL}}$ 480 nm) in the corresponding devices, indicating that the color of electroluminescence could be tuned also through rational structural variations of the ancillary ligands. Here, it is worth noting that the CIE coordinates of devices 5 (0.22, 0.42) and 6 (0.17, 0.38) are very different from each other due to the relatively narrow full spectral width at half-maximum of device 6 (Figure 6b), although they possess the same emission peak at λ_{\max} 480 nm. These data show that the device emission color can be optimized through adjusting the emission bandwidth,¹² which here has been realized by introducing the different substituents (SO₂Me or CF₃) in the ancillary ligand.

Figure 6c–e show the current density–voltage–luminance, external quantum efficiency, and power efficiency–luminance characteristics of the devices 2, 3, 5, and 6. All the devices exhibited a low turn-on voltage (recorded at 1 cd m⁻²), and the EL intensity rises rapidly after the onset voltages. The corresponding maximum luminance values were obtained at rather low voltages, as listed in Table 4. Device 3 exhibited comparable EL efficiency to the reference device 1 based on the similar green emission,¹⁴ while the other devices exhibited higher driving voltages and lower EL efficiencies attributed to the blue shift in emission compared with devices 1 and 3. This is consistent with the known trend of reduced efficiency upon blue-shifting the emission in this spectral region.²⁷ These devices generally realized high efficiencies and insignificant efficiency roll-off. Both the external quantum efficiency (EQE) and power efficiency (PE) values of these devices maintained high levels at luminance values of 10, 100 and 1,000 cd m⁻². Such stable and high EL performance based on the simple device structure suggests that effective charge transport and recombination exists throughout these devices. Notably, devices 2, 3, and 5 reached maximum brightnesses of >26 000 cd m⁻².

CONCLUSIONS

The new complexes 2–6 have been rationally designed and synthesized, and their optoelectronic and structural properties have been characterized, along with their applications as emitters in PhOLEDs. The emission color of photoluminescence and electroluminescence has been tuned via systematic functionalization of both the cyclometalating ligand and the ancillary ligand, which contribute significantly to the frontier orbital distributions. Exchanging the phenylpyridine ligand for 2,4-difluoro-ppy gives a blue shift of 21–22 nm (from 1 to 2 and from 4 to 5), and the introduction of electron-withdrawing substituents (SO₂Me, CF₃) onto the phenoxy ring of the (2'-oxyphenyl)-2-oxazole ligand results in a further blue shift of 13–20 nm. Combining these functionalizations gives a $\lambda_{\max}^{\text{PL}}$ of 476 and 479 for complexes 5 and 6 in dichloromethane solution with PLQYs of ca. 0.7. (TD-)DFT calculations are in excellent agreement with the observed photophysical and electrochemical properties of the complexes. PhOLEDs fabricated from the complexes generally demonstrated high efficiencies and very limited efficiency roll-off. Both the EQE and PE values maintained high levels at luminance values of 10,

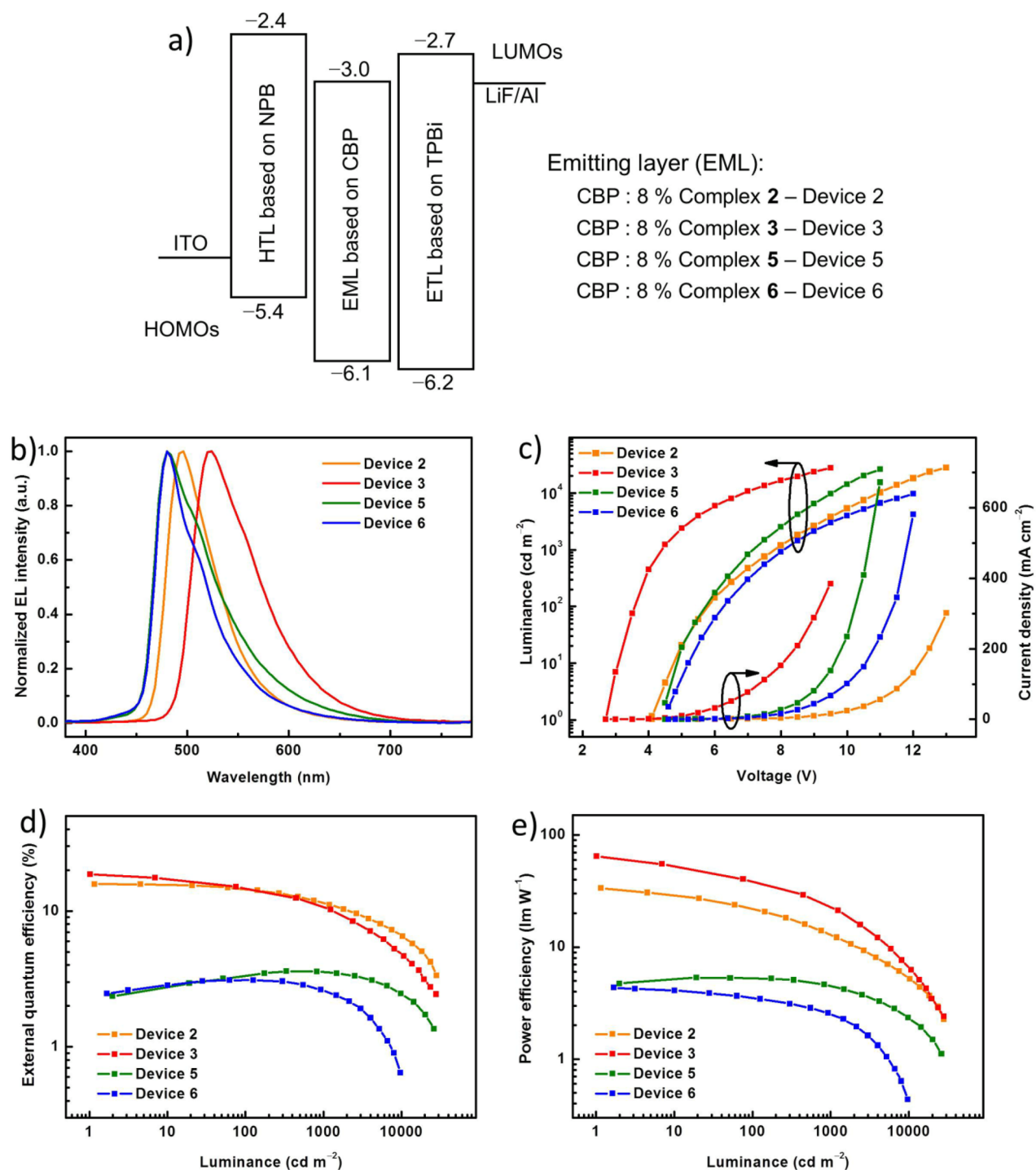


Figure 6. (a) Energy diagram of the devices. (b) EL spectra of the devices at a brightness of 1000 cd m^{-2} . (c) Current density–luminance–driving voltage curves of the devices. (d) EQE–luminance curves of the devices. (e) PE–luminance curves of the devices.

Table 4. Summary of Device Data

device/complex	maximum brightness/ cd m^{-2}	turn-on voltage ^a /V	EQE ^b /%	PE ^b /lm/W	λ_{ELmax} ^c /nm	CIE _{xy} ^c
1 ^d	61 560	3.5	17.7, 17.1, 14.2	47.2, 35.1, 20.8	530	(0.35, 0.61)
2	28 130	4.1	15.6, 14.5, 11.3	28.5, 21.6, 12.7	496	(0.19, 0.53)
3	28 050	2.7	17.3, 14.8, 11.3	52.5, 37.2, 25.5	524	(0.33, 0.61)
5	26 150	4.5	2.6, 3.3, 3.5	5.1, 5.3, 4.5	480	(0.22, 0.42)
6	9670	4.6	2.8, 3.1, 2.6	4.1, 3.5, 2.5	480	(0.17, 0.38)

^aMeasured at a brightness of 1 cd m^{-2} . ^bValues at a brightness of 10, 100, and 1000 cd m^{-2} , respectively. ^cValues at a brightness of 1000 cd m^{-2} .

^dData taken from ref 14.

100, and 1000 cd m⁻², with devices 2, 3, and 5 achieving maximum brightnesses of >26 000 cd m⁻².

Our rational molecular design strategy for tuning the emission color has exploited the unusual frontier orbital distribution in these complexes, namely, a significant HOMO character on the phenoxylate part of the ancillary ligand. Functionalization of an ancillary ligand, as developed in this work, is an attractive complementary approach to the more usual methodology of design and synthesis of different (C[^]N) cyclometalating ligands, where complex formation can be synthetically more challenging for steric and electronic reasons.

EXPERIMENTAL DATA

General Procedures. All commercially available chemicals were used without further purification. Reactions requiring an inert atmosphere were performed under a blanket of argon gas, which was dried over a phosphorus pentoxide column. Anhydrous solvents were dried through an HPLC column on an Innovative Technology Inc. solvent purification system. Column chromatography was performed using 40–60 μm mesh silica gel. Analytical TLC was performed on plates precoated with silica gel (Merck, silica gel 60F₂₅₄) and visualized using UV light (254, 315, 365 nm). NMR spectra were recorded on Bruker Avance 400 MHz, Varian Mercury 200, and 400 MHz, Varian Inova 500 MHz or Varian VNMRS 600 and 700 MHz spectrometers. Chemical shifts are referenced to tetramethylsilane [TMS, Si(CH₃)₄] at 0.00 ppm. Melting points were determined in open-ended capillaries using a Stuart Scientific SMP3 melting point apparatus at a ramping rate of 1 °C/min. They are recorded to the nearest 0.1 °C. ESI and MALDI mass spectra were recorded on a Thermo-Finnigan LTQ FT (7.0 T magnet) spectrometer. ASAP mass spectra were recorded on a Waters Xevo QTOF spectrometer. GCMS spectra were recorded on a Thermo-Finnigan Trace GCMS (EI and CI ion sources). Elemental analyses were obtained on an Exeter Analytical Inc. CE-440 elemental analyzer. Microwave reactions were conducted in a sealed vessel in a Biotage Initiator microwave synthesizer (0–400 W). Where solvent mixtures are mentioned any percentage/ratio is by volume.

Electrochemistry. Cyclic voltammetry data were obtained using a BAS CV50W electrochemical analyzer fitted with a three-electrode system consisting of a Pt disk (Φ = 1.8 mm) as the working electrode, a Pt wire as an auxiliary electrode, and an additional platinum wire as the reference electrode. The experiments were conducted in dry dichloromethane (DCM) solution with ⁿBu₄NPF₆ (0.1 M) as the supporting electrolyte at a scan rate of 100 mV/s. The data were internally referenced to decamethylferrocene, which was then referenced to Fc/Fc⁺ to allow comparison with the literature and estimation of the HOMO levels.

Solution Photophysics. Solution-state photophysical data were obtained using freshly prepared solutions of the complexes in the solvent specified. Emission and lifetime measurements were taken using thoroughly degassed solutions achieved by three freeze–pump–thaw cycles and obtained using a quartz cuvette with a path length of 1 cm. The solutions had an absorbance below 0.10 to minimize inner filter effects. All UV–vis absorption measurements were recorded using a Unicam UV2-100 spectrometer operated with the Unicam Vision (ver. 3.50) software. Baseline correction was achieved by reference to pure solvent in the same cuvette. Absorption measurements were obtained using quartz cuvettes with a path length of 2 cm. Solution PLQYs were recorded in degassed solvent and determined using the relative method, with quinine sulfate (Φ_{PL} = 0.546 in 0.5 M H₂SO₄) as the reference. The PLQYs were computed according to the following equation:

$$\Phi_x = \Phi_{\text{ref}} \frac{\text{Grad}_x}{\text{Grad}_{\text{ref}}} \left(\frac{\eta_x}{\eta_{\text{ref}}} \right)^2$$

where subscripts “x” and “ref” denote the material being measured and the reference, respectively. Φ represents the PLQY, Grad is the

gradient of the gradient from the plot of integrated fluorescence intensity vs absorbance, and η is the refractive index of the solvent. Excitation and emission photoluminescence spectra were recorded on a Horiba Jobin Yvon SPEX Fluorolog 3-22 spectrofluorometer. Quantum yields were determined in degassed DCM in comparison with a standard [quinine sulfate = 0.546 in 0.5 M H₂SO₄]. Solutions of the complexes in degassed DCM [$<10^{-5}$ M] were used for decay measurements. The sample was excited by the output of a pulse laser diode that produced a 1 kHz train of pulses of 20 ns duration at 405 nm. The luminescence was collected at 90° and focused onto the entrance slit of a monochromator (Bethan 300 V). The emission was detected by a photon-counting photomultiplier tube, and the arrival times of photons at the detector were determined using a multichannel scaler.

X-ray Crystallography. X-ray diffraction experiments for **4** and **6** were carried out on a Bruker 3-circle CCD diffractometer D8 Venture with a Photon 100 CMOS area detector, using Mo Kα radiation from an IμS microsource with focusing mirrors and a Cryostream (Oxford Cryosystems) open-flow N₂ gas cryostat. For **2**, the experiment was carried out at room temperature on a Bruker Smart Apex II CCD diffractometer, using Mo Kα radiation (λ = 0.710 69 Å). Structure **4** was solved by Patterson methods, **6** by direct methods using SHELXS 2013/1 software,²⁸ and **2** by direct methods using SIR2002 software.²⁹ The structures were refined in anisotropic approximation by full matrix least-squares against F² off all data, using OLEX2³⁰ and SHELXL 2014/7 software.³¹ The asymmetric unit of **4** contains one complex molecule and two molecules of THF, one of them partly disordered. The asymmetric unit of **6** contains two complex molecules (both with rotationally disordered CF₃ groups) and one disordered solvent molecule. Presumably, the latter site is shared by DCM and CDCl₃ molecules in a 0.8:0.2 ratio. The asymmetric unit of **2** contains one complex molecule and half of one DCM molecule, the latter having crystallographic C₂ symmetry.

Thermal Analysis. Thermogravimetric analysis was performed in a nitrogen atmosphere using a PerkinElmer Pyris 1 TGA instrument. The complexes were heated at a rate of 10 °C/min from room temperature up to 600 °C.

Synthesis and Characterization. Iridium Complex 2. IrCl₃·3H₂O (209 mg, 0.59 mmol) was added to a stirred solution of 2-(2,4-difluorophenyl)pyridine (250 mg, 1.31 mmol) in 2-ethoxyethanol (6 mL) under argon. The solution was heated to 135 °C for 6 h before 2-(2'-hydroxyphenyl)-2-oxazoline (**21**)^{14,19} (121 mg, 0.74 mmol) and Na₂CO₃ (315 mg, 2.97 mmol) were added, and the solution was heated at 135 °C overnight. Water was added and the yellow precipitate was collected by filtration. The residue was purified by column chromatography (hexane/EtOAc, 4:1) to give complex **2** as a yellow solid (310 mg, 79%). Anal. Calcd for C₃₁H₂₀F₄IrN₃O₂: C, 50.68; H, 2.74; N, 5.72. Found: C, 50.43; H, 3.07; N, 5.47. δ_H (400 MHz; CD₂Cl₂) 8.78 (1H, d, J 5.2), 8.39 (1H, d, J 5.8), 8.26 (2H, t, J 8.9), 7.87–7.75 (2H, m), 7.61 (1H, d, J 8.1), 7.21 (1H, t, J 6.6), 7.14 (2H, t, J 7.0), 6.60 (1H, d, J 8.7), 6.45–6.32 (3H, m), 5.79 (1H, dd, J 8.9, 2.3), 5.62 (1H, dd, J 8.9, 2.4), 4.36 (1H, q, J 9.3), 4.23 (1H, q, J 8.5), 3.64–3.47 (1H, m), 3.14–3.00 (1H, m); δ_F (376 MHz CD₂Cl₂) –109.30 (1F, q, J 9.1), –109.34 (1F, q, J 9.3), –110.90 (1F, ddd, J 12.4, 10.1, 1.6), –110.95 (1F, ddd, J 12.5, 10.1, 2.5). HRMS (FTMS +ESI): calcd for [C₃₁H₂₀F₄N₃O₂Ir+H]⁺ 734.1176, found 734.1186. Crystals for X-ray analysis were grown by slow evaporation of a DCM/methanol solution of **2**.

N-(2,2-Diethoxyethyl)-2-methoxybenzamide, 8. Methyl-2-methoxybenzoate (**7**) (5.00 g, 28.93 mmol) and aminoacetaldehyde diethylacetal (2.78 g, 17.25 mmol) were combined, and the mixture was heated to 160 °C for 4 h before being cooled to RT. An NMR spectrum of the crude material showed the reaction had not gone to completion; more aminoacetaldehyde diethylacetal (1.00 g, 6.20 mmol) was added, and the reaction was heated to 160 °C overnight before being cooled to RT. Any methanol produced was removed by rotary evaporation, and the oily residue was purified by column chromatography (hexane/EtOAc, 1:1) to give an oil, N-(2,2-diethoxyethyl)-2-methoxybenzamide (**8**) (2.80 g, 36%): δ_H (400 MHz; CDCl₃) 8.21 (1H, dd, J 7.8, 1.9), 8.15 (1H, br t, J 5.5), 7.45

(1H, ddd, J 8.3, 7.3, 1.8), 7.08 (1H, ddd, J 7.8, 7.3, 1.0), 6.98 (1H, dd, J 8.4, 1.0), 4.63 (1H, t, J 5.6), 3.97 (3H, s), 3.76 (dq, J 9.4, 7.0), 3.67–3.54 (4H, m), 1.25 (6H, t, J 7.0). HRMS (FTMS+ESI): calcd for $[C_{14}H_{21}NO_4+Na]^+$ 290.1368, found 290.1368. The ^{13}C NMR spectrum could not be obtained as **8** hydrolyzed to the aldehyde in the NMR solvent; δ_H (600 MHz; $CDCl_3$) 9.76 (1H, d, J 0.6), 8.64 (1H, br s), 8.21 (1H, dd, J 7.7, 1.9), 7.51–7.45 (1H, m), 7.09 (1H, t, J 7.6), 7.01 (1H, d, J 8.4), 4.41 (2H, dd, J 4.8, 0.7), 4.03 (3H, d, J 0.6); δ_C (151 MHz; $CDCl_3$) 196.97, 165.69, 157.96, 133.45, 132.52, 121.48, 120.70, 111.55, 56.20, 51.15.

2-(2-Methoxyphenyl)oxazole (9) and 2-(2-Methoxy-5-(methylsulfonyl)phenyl)oxazole (10). Methanesulfonic acid (35 mL) was added cautiously to *N*-(2,2-diethoxyethyl)-2-methoxybenzamide (**8**) (2.80 g, 11.70 mmol) with stirring. P_4O_{10} (4.50 g, 5.85 mmol) was added with caution, and the mixture was heated to 180 °C overnight. The mixture was cooled to RT and added dropwise to an aqueous $NaHCO_3$ solution (300 mL) with stirring. The aqueous phase (pH 8) was extracted with DCM (3 × 400 mL), and the solvent was removed *in vacuo* to leave a thick oil. The residue was purified by column chromatography (10–20% EtOAc in DCM) to give the product **9** as a yellow oil (400 mg, 19%): δ_H (400 MHz; $CDCl_3$) 7.98 (1H, dd, J 8.1, 1.8), 7.76 (1H, d, J 0.8), 7.46 (1H, ddd, J 8.3, 7.4, 1.8), 7.31 (1H, d, J 0.8), 7.04–7.11 (2H, m), 4.00 (3H, s); δ_C (151 MHz; $CDCl_3$) 160.44, 157.67, 138.31, 131.90, 130.41, 128.28, 120.79, 116.61, 112.10, 56.20; HRMS (FTMS+ESI) calcd for $[C_{10}H_9NO_2+H]^+$ 176.0712, found 176.0740.

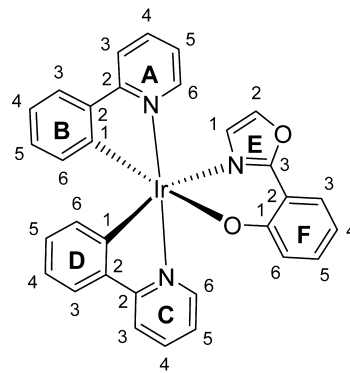
Also isolated was a second fraction: 2-(2-methoxy-5-(methylsulfonyl)phenyl)oxazole (**10**) (538 mg, 18%): δ_H (400 MHz; $CDCl_3$) 8.54 (1H, dd, J 2.4, 0.8), 8.01 (1H, ddd, J 8.8, 2.4, 0.8), 7.78 (1H, d, J 0.8), 7.33 (1H, s), 7.18 (1H, d, J 8.8), 4.07 (3H, s), 3.09 (3H, s); δ_C (151 MHz; $CDCl_3$) 161.29, 158.31*, 139.10, 131.21, 130.18, 128.69, 117.36*, 112.49, 56.85, 44.94 (* denotes carbons identified from the HMBC spectrum). One carbon is not observed due to low solubility. HRMS (FTMS+ESI): calcd for $[C_{11}H_{11}NO_4S+H]^+$ 254.0487, found 254.0471.

2-(Oxazol-2-yl)phenol, 11. BBr_3 (0.65 mL, 6.87 mmol) was added dropwise to a stirred solution of 2-(2-methoxyphenyl)oxazole (**9**) (400 mg, 2.28 mmol) in DCM (10 mL, dry) over an ice bath. The suspension was stirred at RT overnight before the reaction was quenched with water (CAUTION). The solid formed, presumed to be 2-(2-hydroxyphenyl)oxazol-3-ium bromide was filtered off and suspended in DCM. This was then washed with aqueous Na_2CO_3 to neutralize the salt. The organic phase was collected, and the aqueous phase was washed with further DCM (3 × 50 mL). The organic phases were combined, dried over $MgSO_4$, and filtered. The solvent was removed *in vacuo* to give an oil, 2-(oxazol-2-yl)phenol (**11**) (250 mg, 68%): δ_H (700 MHz; $CDCl_3$) 11.20 (1H, s), 7.84 (1H, dd, J 7.8, 1.7), 7.69 (1H, t, J 0.9), 7.39–7.34 (1H, m), 7.24 (1H, d, J 1.0), 7.08 (1H, dd, J 8.3, 1.2), 6.95 (1H, td, J 7.5, 1.0); δ_C (176 MHz; $CDCl_3$) 161.78, 157.35, 137.49, 132.47, 126.51, 126.08, 119.52, 117.31, 111.25. HRMS (FTMS+ESI): calcd for $[C_9H_7NO_2+H]^+$ 162.0555, found 162.0542.

4-(Methylsulfonyl)-2-(oxazol-2-yl)phenol, 12. BBr_3 (0.61 mL, 6.37 mmol) was added dropwise to a stirred solution of 2-(2-methoxy-5-(methylsulfonyl)phenyl)oxazole (**10**) (538 mg, mmol) in DCM (10 mL, dry) over an ice bath. The suspension was stirred at RT overnight before the reaction was quenched with water (CAUTION). The solid formed, presumed to be 2-(2-hydroxy-5-(methylsulfonyl)phenyl)oxazol-3-ium bromide, was filtered off and suspended in DCM. This was then washed with aqueous Na_2CO_3 to neutralize the salt. The organic phase was collected, and the aqueous phase was washed with further DCM (3 × 50 mL). The organic phases were combined, dried over $MgSO_4$, and filtered. TLC revealed a mixture of starting material and product; the crude mixture was redissolved in DCM and extracted with aqueous $NaOH$ solution (3 × 50 mL, 1 M). The aqueous phases were combined, acidified to pH 6 with concentrated HCl, and re-extracted with DCM (4 × 100 mL). The organic phase was dried over $MgSO_4$, the solvent was removed, and the residue was purified by silica plug (EtOAc) to give a white solid, 4-(methylsulfonyl)-2-(oxazol-2-yl)phenol (**12**) (200 mg, 39%), which was recrystallized from

methanol: δ_H (400 MHz; $CDCl_3$) 11.91 (1H, s), 8.47 (1H, d, J 2.4), 7.91 (1H, dd, J 8.8, 2.4), 7.79 (1H, d, J 0.9), 7.32 (1H, d, J 0.9), 7.23 (1H, d, 8.8), 3.10 (3H, s); δ_C (101 MHz; $CDCl_3$) 161.39, 160.21, 138.54, 131.68, 131.30, 126.78, 126.56, 118.56, 111.65, 45.01. HRMS (FTMS+ESI): calcd for $[C_{10}H_9NO_4S]^+$ 240.0331, found 240.0335.

Iridium Complex 3. $IrCl_3 \cdot 3H_2O$ (123 mg, 0.35 mmol) was added to a stirred solution of 2-phenylpyridine (0.11 mL, 0.77 mmol) in 2-ethoxyethanol (10 mL). The solution was heated to reflux (135 °C) overnight. Na_2CO_3 (300 mg, 2.83 mmol) and 2-(oxazol-2-yl)phenol (**11**) (62 mg, 0.38 mmol) were added, and the solution was heated to reflux overnight before being cooled to RT. Water was added, and the precipitate was filtered to give a yellow solid. The crude product was filtered and washed with more water to remove water-soluble impurities. The product was dried, then washed with hexane and cold diethyl ether to remove traces of ppy ligand. The product was obtained as a yellow solid, **3** (200 mg, 87%). Anal. Calcd for $C_{31}H_{22}IrN_3O_2 \cdot 0.25CH_2Cl_2$: C, 55.00; H, 3.33; N, 6.17. Found: C, 55.18; H, 3.26; N, 6.02. δ_H (700 MHz; $CDCl_3$) 8.88 (1H, d, J 5.7, H_{A6}), 7.99 (1H, d, J 5.8, H_{C6}), 7.85 (1H, d, J 8.2, H_{C3}), 7.80 (1H, d, J 8.2, H_{A3}), 7.72 (1H, dd, J 8.2, 1.9, H_{F3}), 7.67 (1H, td, J 8.1, 1.5, H_{A4}), 7.65 (1H, td, J 8.1, 1.5, H_{C4}), 7.59 (1H, dd, J 7.9, 1.1, H_{D3}), 7.56 (1H, dd, J 7.6, 1.1, H_{B3}), 7.38 (1H, d, J 1.0, H_{E2}), 7.12 (1H, ddd, J 8.7, 7.0, 1.9, H_{F5}), 7.07 (1H, ddd, J 7.4, 6.0, 1.4, H_{A5}), 6.92 (1H, ddd, J 8.1, 5.9, 1.4, H_{C5}), 6.87 (1H, td, J 7.5, 1.2, H_{D4}), 6.86 (1H, td, J 7.4, 1.2, H_{B4}), 6.80–6.75 (2H, m, H_{F6+D5}), 6.73 (1H, dt, J 7.3, 1.1, H_{B5}), 6.42 (1H, ddd, J 7.9, 6.9, 1.1, H_{F4}), 6.36 (1H, d, J 7.6, H_{B6}), 6.28 (1H, d, J 7.6, H_{D6}), 6.20 (1H, d, J 1.0, H_{E1}); δ_C (151 MHz; $CDCl_3$) 169.22 (C_{C2}), 168.10 (C_{A2}), 167.20 (C_{F1}), 158.67 (C_{E3}), 152.67 (C_{D1}), 149.07 (C_{A6}), 148.72 (C_{B1}), 148.67 (C_{C6}), 144.87 (C_{B2}), 144.83 (C_{D2}), 137.49 (C_{E2}), 136.91 (C_{A4}), 136.74 (C_{C4}), 133.20 (C_{B6}), 132.56 (C_{F5}), 132.48 (C_{D6}), 129.69 (C_{B5}), 129.58 (C_{D5}), 127.39 (C_{F3}), 126.64 (C_{E1}), 125.53 (C_{F6}), 124.18 (C_{B3}), 124.10 (C_{D3}), 122.07 (C_{A5}), 121.80 (C_{C5}), 120.79 (C_{D4}), 119.02 (C_{B4}), 118.73 (C_{C3}), 118.25 (C_{A3}), 113.34 (C_{F4}), 110.94 (C_{E2}). HRMS (FTMS+ESI): calcd for $[C_{31}H_{22}N_3O_4^{191}Ir+H]^+$ 660.1396, found 660.1406.



Iridium Complex 4. $IrCl_3 \cdot 3H_2O$ (236 mg, 0.67 mmol) was added to a stirred solution of 2-phenylpyridine (0.21 mL, 1.47 mmol) in 2-ethoxyethanol (10 mL). The solution was heated to reflux (135 °C) overnight. Na_2CO_3 (354 mg, 3.34 mmol) and 4-(methylsulfonyl)-2-(oxazol-2-yl)phenol (**12**) (200 mg, 0.84 mmol) were added, and the solution was heated to reflux overnight before being cooled to RT. Water was added and the precipitate was filtered to give a yellow solid. The crude material was purified by column chromatography (10% EtOAc in DCM) to give the product as a yellow solid. Fractions containing product **4** contaminated with unreacted ppy were combined, the solvent was then removed, and the solid was washed with hexane to give additional product **4** (combined yield: 281 mg, 57%). Anal. Calcd for $C_{32}H_{24}IrN_3O_4S$: C, 52.02; H, 3.27; N, 5.69. Found: C, 51.84; H, 3.61; N, 5.27. δ_H (400 MHz; $CDCl_3$) 8.75 (1H, ddd, J 5.8, 1.5, 0.7), 8.38 (1H, d, J 2.6), 7.96 (1H, d, J 5.7, 1.5, 0.7), 7.91 (1H, d, J 8.1), 7.87 (1H, d, J 8.1), 7.75 (1H, td, J 7.6, 1.7), 7.73 (1H, td, J 7.5, 1.6), 7.60 (1H, td, J 8.4, 1.1), 7.57 (1H, dd, J 9.2, 2.6), 7.49 (1H, d, J 1.0), 7.14 (1H, ddd, J 7.3, 5.7, 1.4), 7.01 (1H, ddd, J 7.4, 5.8, 1.5), 6.93 (1H, td, J 7.5, 1.2), 6.92 (1H, td, J 7.5, 1.2), 6.82 (1H, d, J 9.2), 6.79 (1H, td, J 6.16, 1.2), 6.76 (1H, td, J 7.4, 1.4), 6.83–6.77

(1H, m), 6.79–6.74 (m, 1H), 6.38 (1H, dd, *J* 7.7, 1.0), 6.29 (1H, dd, *J* 7.6, 1.0), 6.27 (1H, d, *J* 1.0), 3.04 (s, 3H). HRMS (FTMS+ESI): calcd for $[C_{32}H_{24}N_3O_4S^{191}Ir]^+$ 737.1094, found 737.1118. Crystals for X-ray analysis were grown by slow evaporation of a solution of **4** in tetrahydrofuran.

N-(2,2-Diethoxyethyl)-2-methoxy-5-(methylsulfonyl)benzamide, **15**. $SOCl_2$ (15 mL) was added to 2-methoxy-5-(methylsulfonyl)benzoic acid (**13**) (6.00 g, 26.06 mmol), and the mixture was heated to reflux under a nitrogen atmosphere for 3 h, before being cooled to RT. The excess $SOCl_2$ was removed *in vacuo* to leave an off-white solid, 2-methoxy-5-(methylsulfonyl)benzoyl chloride, which was used without further purification. A solution of 2-methoxy-5-(methylsulfonyl)benzoyl chloride in DCM (20 mL) was added dropwise to a stirred solution of aminoacetaldehyde diethylacetal (4.16 mL, 28.66 mmol) and NEt_3 (0.33 mL, 28.66 mmol) in DCM (40 mL). The reaction was left to stir at RT overnight. The solvent was removed *in vacuo*, and solid was then suspended in water and sonicated, followed by stirring. The product was then collected via filtration. This washing was repeated a second time, and the product was collected as a white solid, *N*-(2,2-diethoxyethyl)-2-methoxy-5-(methylsulfonyl)benzamide (**15**) (7.25 g, 81%): δ_H (400 MHz; $CDCl_3$) 8.77 (1H, d, *J* 2.6), 8.04 (1H, dd, *J* 8.7, 2.6), 7.94 (1H, s), 7.13 (1H, d, *J* 8.8), 4.63 (1H, t, *J* 5.4), 4.07 (3H, s), 3.76 (2H, dq, *J* 9.4, 7.1), 3.67–3.53 (4H, m), 3.06 (3H, s), 1.25 (6H, t, *J* 7.0); δ_C (101 MHz; $CDCl_3$) 163.49, 161.14, 133.64, 132.39, 132.09, 122.90, 112.13, 100.86, 63.02, 56.77, 44.66, 42.60, 15.53; the molecular ion was not observed and the product was characterized by fragment ions, MS (ASAP+): $[M - OEt]^+ = 300.1$ $[M - NHCH_2CH(OEt)_2]^+ = 213.0$.

N-(2,2-Diethoxyethyl)-2-methoxy-5-trifluoromethylbenzamide, **16**. $SOCl_2$ (7 mL) was added to 2-methoxy-5-(trifluoromethyl)benzoic acid (**14**) (1.37 g, 6.22 mmol), and the mixture was heated to reflux under a nitrogen atmosphere for 3 h, before being cooled to RT. The excess $SOCl_2$ was removed *in vacuo* to leave an off-white solid, 2-methoxy-5-trifluoromethylbenzoyl chloride, which was used without further purification. A solution of 2-methoxy-5-trifluoromethylbenzoyl chloride in DCM (5 mL) was added dropwise to a stirred solution of aminoacetaldehyde diethylacetal (1.00 mL, 6.84 mmol) and NEt_3 (0.95 mL, 6.84 mmol) in DCM (20 mL). The reaction was stirred at RT overnight, before the solvent was removed *in vacuo*. The resulting solid was then suspended in water and sonicated, followed by stirring. The product was then collected via filtration. This was repeated a second time, and the product was collected as a white solid, *N*-(2,2-diethoxyethyl)-2-methoxy-5-trifluoromethylbenzamide (**16**) (2.00 g, 97%): δ_H (400 MHz; $CDCl_3$) 8.51 (1H, d, *J* 2.5), 8.04 (1H, br s), 7.70 (1H, ddd, *J* 8.7, 2.6, 0.8), 7.07 (1H, d, *J* 8.7), 4.63 (1H, t, *J* 5.4), 4.03 (3H, s), 3.76 (2H, dq, *J* 9.4, 7.0), 3.67–3.53 (4H, m), 1.25 (6H, t, *J* 7.0); δ_F (376 MHz; $CDCl_3$) –61.89 (3F, d, *J* 0.8); δ_C (101 MHz; $CDCl_3$) 164.06, 159.77, 130.16 (q, *J* 3.8), 129.83 (q, *J* 3.8), 124.08 (q, *J* 272.1), 123.96 (q, *J* 32.3), 122.10, 111.76, 100.99, 63.01, 56.48, 42.58, 15.54. HRMS (FTMS+ESI): calcd for $[C_{15}H_{20}F_3NO_4+Na]^+$ 358.1242, found 358.1245.

2-Methoxy-5-(methylsulfonyl)-*N*-(2-oxoethyl)benzamide, **17**. Dilute HCl (2 drops, 2 M) was added to a stirred solution of *N*-(2,2-diethoxyethyl)-2-methoxy-5-(methylsulfonyl)benzamide (**15**) (2.00 g, 5.79 mmol) in acetone/water (60 mL/20 mL), and the mixture was heated to reflux for 5 h before stirring at RT overnight. The solvent was removed *in vacuo* to give the product, 2-methoxy-5-(methylsulfonyl)-*N*-(2-oxoethyl)benzamide (**17**) (1.57 g, 100%): δ_H (400 MHz; $CDCl_3$) 9.78 (1H, s), 8.77 (1H, d, *J* 2.5), 8.49 (1H, br s), 8.07 (1H, dd, *J* 8.8, 2.5), 7.17 (1H, d, *J* 8.8), 4.46 (2H, d, *J* 4.7), 4.14 (3H, s), 3.07 (3H, s); δ_C (101 MHz; $CDCl_3$) 196.11, 163.56, 161.37, 133.77, 132.57, 132.53, 122.04, 112.30, 57.00, 51.28, 44.70. HRMS (FTMS+ESI): calcd for $[C_{11}H_{13}NO_5S+H]^+$ 272.0593, found 272.0606.

2-Methoxy-*N*-(2-oxoethyl)-5-(trifluoromethyl)benzamide, **18**. HCl (2 drops, 2 M) was added to a stirred solution of *N*-(2,2-diethoxyethyl)-2-methoxy-5-trifluoromethylbenzamide (**16**) (2.00 g, 5.96 mmol) in acetone/water (30 mL/10 mL), and the mixture was heated to reflux for 4 h before being stirred at RT overnight. The solvent was removed *in vacuo* to give the product, 2-methoxy-*N*-(2-

oxoethyl)-5-(trifluoromethyl)benzamide (**18**) (1.56 g, 100%): δ_H (400 MHz; $CDCl_3$) 9.78 (1H, s), 8.57 (1H, br s), 8.51 (1H, d, *J* 2.4), 7.73 (1H, ddd, *J* 8.7, 2.5, 0.8), 7.11 (1H, d, *J* 8.7), 4.45 (2H, d, *J* 4.7), 4.10 (3H, s); δ_F (376 MHz; $CDCl_3$) –61.92 (3F, s); δ_C (176 MHz; $CDCl_3$) 196.3, 164.17, 160.00 (d, *J* 0.9), 130.31 (q, *J* 3.8), 130.21 (q, *J* 3.8), 124.04 (q, *J* 32.1), 124.03 (q, *J* 271.6), 121.23, 111.90, 56.69, 51.25. HRMS (FTMS+ESI): calcd for $[C_{11}H_{10}NO_3F_3+H]^+$ 262.0691, found 262.0693

2-(2-Methoxy-5-(methylsulfonyl)phenyl)oxazole, **10**. Burgess' reagent (2.07 g, 8.69 mmol) was added to a solution of 2-methoxy-5-(methylsulfonyl)-*N*-(2-oxoethyl)benzamide (**17**) (1.57 g, 5.79 mmol) in THF (15 mL) in a 20 mL microwave vial. The reaction was heated to 70 °C in the microwave for 10 min with stirring. Once cooled, the solvent was removed and the residue purified by column chromatography (EtOAc) to give the product, 2-(2-methoxy-5-(methylsulfonyl)phenyl)oxazole (**10**) (0.30 g, 20%); NMR data were consistent with the sample obtained previously (see above).

Iridium Complex **5**. $IrCl_3 \cdot 3H_2O$ (120 mg, 0.34 mmol) was added to a solution of *dfppy* (143 mg, 0.75 mmol) in 2-ethoxyethanol (5 mL), and the mixture was heated to 130 °C overnight under a nitrogen atmosphere. The mixture was cooled, and Na_2CO_3 (180 mg, 1.70 mmol) and 4-(methylsulfonyl)-2-(oxazol-2-yl)phenol (**12**) (102 mg, 0.43 mmol) were added. The solution was heated to reflux overnight under a nitrogen atmosphere, before being cooled to RT, and the solvent removed *in vacuo*. The residue was purified by column chromatography (hexane/acetone, 2:1). The solid obtained was dissolved in methanol and triturated with hexane to give the product as a yellow solid (197 mg, 71%). Anal. Calcd for $C_{32}H_{20}IrN_3O_4F_4S$: C, 47.40; H, 2.49; N, 5.18. Found: C, 47.00; H, 2.56; N, 5.07. δ_H (400 MHz; acetone- d_6) 8.76 (1H, ddd, *J* 5.8, 1.7, 0.8), 8.36–8.26 (4H, m), 8.09–7.97 (3H, m), 7.56 (1H, dd, *J* 9.1, 2.6), 7.44 (1H, ddd, *J* 7.4, 5.8, 1.4), 7.28 (1H, ddd, *J* 7.4, 5.8, 1.5), 6.68 (1H, d, *J* 9.1), 6.60 (1H, ddd, *J* 12.8, 9.4, 2.4), 6.56 (1H, ddd, *J* 12.8, 9.4, 2.4), 6.46 (1H, d, *J* 1.1), 5.84 (1H, dd, *J* 8.8, 2.4), 5.67 (1H, dd, *J* 8.9, 2.4), 3.03 (3H, s); δ_F (376 MHz; acetone- d_6) –109.37 (1F, q, *J* 9.4), –110.28 (1F, q, *J* 9.5), –111.32 (1F, t, *J* 11.5), –112.06 (1F, t, *J* 11.3). HRMS (FTMS+ESI): calcd for $[C_{32}H_{20}N_3O_4F_4S^{191}Ir+H]^+$ 810.0795, found 810.0803.

2-(2-Methoxy-5-(trifluoromethyl)phenyl)oxazole, **19**. Burgess' reagent (0.43 g, 1.80 mmol) was added to a solution of 2-methoxy-*N*-(2-oxoethyl)-5-(trifluoromethyl)benzamide (**18**) (0.24 g, 0.92 mmol) in THF (4 mL) in a 2–5 mL microwave vial. Five vials were set up, and the reactions were heated to 70 °C in the microwave for 10 min with stirring. Once cooled, the solutions were combined and the solvent was removed. The residue was purified by column chromatography (initially DCM, changed to 10% EtOAc in DCM) to give the product, 2-(2-methoxy-5-(trifluoromethyl)phenyl)oxazole (**19**) (440 mg, 40%): δ_H (400 MHz; $CDCl_3$) 8.24 (1H, d, *J* 2.4), 7.77 (1H, d, *J* 0.8), 7.68 (1H, ddd, *J* 8.8, 2.5, 0.8), 7.32 (1H, d, *J* 0.8), 7.12 (1H, d, *J* 8.8), 4.03 (3H, s); δ_F (376 MHz; $CDCl_3$) –61.80 (3F, d, *J* 0.8); δ_C (101 MHz; $CDCl_3$) 159.77, 159.13, 138.85, 128.76 (q, *J* 3.8), 128.62, 127.79 (q, *J* 3.8), 124.11 (q, *J* 271.0), 123.23 (q, *J* 33.1), 117.00, 112.14, 56.54. HRMS (FTMS+ESI): calcd for $[C_{11}H_8NO_2F_3+H]^+$ 244.0585, found 244.0580.

4-(Trifluoromethyl)-2-(oxazol-2-yl)phenol, **20**. 2-(2-Methoxy-5-(trifluoromethyl)phenyl)oxazole (**19**) (440 mg, 1.81 mmol) was added to molten pyridine hydrochloride (8.00 g, 69.22 mmol) at 160 °C. The reaction was heated at 160 °C for 6 h before being cooled to RT. Water (40 mL) and EtOAc (40 mL) were added, and the layers were separated. The organic layer was washed with further water (3 × 50 mL), then dried over $MgSO_4$, and the solvent removed *in vacuo*. The residue was purified by column chromatography (DCM) to give a mixture of the product, 4-(trifluoromethyl)-2-(oxazol-2-yl)phenol (**20**), and a decomposition product (102 mg). δ_H (400 MHz; $CDCl_3$) 11.60 (1H, s), 8.15 (1H, d, *J* 2.0), 7.78 (1H, d, *J* 0.9), 7.62 (1H, ddd, *J* 8.7, 2.3, 0.7), 7.32 (1H, d, *J* 0.9), 7.18 (1H, d, *J* 8.6); δ_F (376 MHz; $CDCl_3$) –62.01 (3F, s). HRMS (FTMS+ESI): calcd for $[C_{10}H_6NO_2F_3+H]^+$ 230.0429, found 230.0423.

The decomposition product was identified by NMR and mass spectrometry as 2-hydroxy-5-(trifluoromethyl)benzamide.

Iridium Complex 6. IrCl₃·3H₂O (170 mg, 0.41 mmol) was added to a solution of dfppy (170 mg, 0.89 mmol) in 2-ethoxyethanol (5 mL), and the mixture was heated to 130 °C overnight under a nitrogen atmosphere. The mixture was cooled, and Na₂CO₃ (214 mg, 2.02 mmol) and 2-(2-methoxy-5-(trifluoromethyl)phenyl)oxazole (**20**) (102 mg, 0.45 mmol) were added. The solution was heated to reflux overnight under a nitrogen atmosphere, before being cooled to RT, and the solvent removed *in vacuo*. The residue was purified by column chromatography (hexane/EtOAc, 2:1) to give the product as a yellow solid, complex **6** (160 mg, 50%). Anal. Calcd for C₃₂H₁₇IrN₃O₂F₇: C, 48.00; H, 2.14; N, 5.25. Found: C, 48.53; H, 2.31; N, 5.18. δ_H (400 MHz; acetone-*d*₆) 8.79 (1H, ddd, *J* 5.7, 1.7, 0.8), 8.36–8.26 (3H, m), 8.09–7.96 (4H, m), 7.43 (1H, ddd, *J* 7.3, 5.8, 1.4), 7.35 (1H, dd, *J* 9.1, 2.6), 7.27 (1H, ddd, *J* 7.4, 5.8, 1.5), 6.69 (1H, d, *J* 8.9), 6.57 (2H, dddd, *J* 18.7, 12.8, 9.4, 2.4), 6.44 (1H, d, *J* 1.1), 5.85 (1H, dd, *J* 8.8, 2.4), 5.67 (1H, dd, *J* 8.8, 2.4), 2.81–2.75 (2H, m), 2.09 (3H, s); δ_F (376 MHz; acetone-*d*₆) –61.42 (3F, m), –109.45 (1F, q, *J* 9.4), –110.37 (1F, q, *J* 9.4), –111.38 (1F, t, *J* 11.5), –112.14 (1F, ddd, *J* 12.4, 9.9, 1.7). HRMS (FTMS+ESI): calcd for [C₃₂H₁₇N₃O₂F₇¹⁹¹Ir + H]⁺ 800.0893, found 800.0883. Crystals for X-ray analysis were grown by slow evaporation of a DCM/CDCl₃/hexane solution of **6** in an NMR tube.

■ ASSOCIATED CONTENT

● Supporting Information

The Supporting Information is available free of charge on the ACS Publications website at DOI: 10.1021/acs.organomet.7b00161.

NMR spectra and additional computational, photo-physical, and electrochemical data (PDF)

X-ray crystallographic data (CIF)

Cartesian coordinates of optimized geometries (PDF)

■ AUTHOR INFORMATION

Corresponding Authors

*E-mail: yuliu@jlu.edu.cn.

*E-mail: zhudx047@nenu.edu.cn.

*E-mail: m.r.bryce@durham.ac.uk.

ORCID

Yu Liu: 0000-0001-8686-1503

Andrei S. Batsanov: 0000-0002-4912-0981

Martin R. Bryce: 0000-0003-2097-7823

Notes

The authors declare no competing financial interest.

Crystal data have been deposited with the Cambridge Crystallographic database as CCDC numbers 1512945–1592947.

■ ACKNOWLEDGMENTS

We thank Durham University for a doctoral scholarship (to H.B.), EPSRC grant EP/K039423/1 for funding work in Durham, and NSFC (Nos. 51373062, 51473028), the Key Scientific and Technological Project of Jilin Province (20150204011GX, 20160307016GX), and the Development and Reform Commission of Jilin Province (20160058) in China.

■ REFERENCES

- (1) Yam, V. W.-W.; Wong, K. M.-C. *Chem. Commun.* **2011**, 47, 11579–11592.
- (2) (a) Liu, S.; Zhou, N.; Chen, Z.; Wei, H.; Zhu, Y.; Guo, S.; Zhao, Q. *Opt. Lett.* **2017**, 42, 13–16. (b) Liu, S.; Zhang, Y.; Liang, H.; Chen, Z.; Liu, Z.; Zhao, Q. *Opt. Express* **2016**, 24, 15757–15764. (c) Liu, S.; Xu, A.; Chen, Z.; Ma, Y.; Yang, H.; Shi, Z.; Zhao, Q. *Opt. Express* **2016**, 24, 28247–28255.
- (3) Sun, H.; Liu, S.; Lin, W.; Zhang, K. Y.; Lv, W.; Huang, X.; Huo, F.; Yang, H.; Jenkins, G.; Zhao, Q.; Huang, W. *Nat. Commun.* **2014**, 5, 3601–3610.
- (4) (a) Luminescent Complexes and Materials for Light-Emitting Devices: Themed Issue. *Dalton Trans.* **2015**, 44, 8317–8317. (b) Mertens, R. *The OLED Handbook. A Guide to OLED Technology, Industry and Market*; 2014: www.oled-info.com/handbook. (c) Yang, X.; Zhou, G.; Wong, W.-Y. *Chem. Soc. Rev.* **2015**, 44, 8484–8575. (d) Xiao, L.; Chen, Z.; Qu, B.; Luo, J.; Kong, S.; Gong, Q.; Kido, J. *Adv. Mater.* **2011**, 23, 926–952. (e) Cloy, W. C. H.; Chan, W. K.; Yuan, Y. *Adv. Mater.* **2014**, 26, 5368–5399.
- (5) (a) Kamtekar, K. T.; Monkman, A. P.; Bryce, M. R. *Adv. Mater.* **2010**, 22, 572. (b) Ying, L.; Ho, C.-L.; Wu, H.; Cao, Y.; Wong, W.-Y. *Adv. Mater.* **2014**, 26, 2459–2473.
- (6) (a) Baldo, M. A.; Thompson, M. E.; Forrest, S. R. *Nature* **2000**, 403, 750–753. (b) Lamansky, S.; Djurovich, P.; Murphy, D.; Abdel-Razzaq, F.; Lee, H.-E.; Adachi, C.; Burrows, P. E.; Forrest, S. R.; Thompson, M. E. *J. Am. Chem. Soc.* **2001**, 123, 4304–4312.
- (7) Chou, P. T.; Chi, Y. *Chem. - Eur. J.* **2007**, 13, 380–395.
- (8) (a) Ladouceur, S.; Zysman-Colman, E. *Eur. J. Inorg. Chem.* **2013**, 2013, 2985–3007. (b) You, Y.; Park, S. Y. *Dalton Trans.* **2009**, 1267–1282.
- (9) Rausch, A. F.; Thompson, M. E.; Yersin, H. *J. Phys. Chem. A* **2009**, 113, 5927–5932.
- (10) Baranoff, E.; Curchod, B. F. *Dalton Trans.* **2015**, 44, 8318–8329.
- (11) Sajoto, T.; Djurovich, P. I.; Tamayo, A.; Yousufuddin, M.; Bau, R.; Thompson, M. E.; Holmes, R. J.; Forrest, S. R. *Inorg. Chem.* **2005**, 44, 7992–8003.
- (12) Yang, C.-H.; Mauro, M.; Polo, F.; Watanabe, S.; Muenster, I.; Fröhlich, R.; De Cola, L. *Chem. Mater.* **2012**, 24, 3684–3695.
- (13) You, Y.; Kim, K. S.; Ahn, T. K.; Kim, D.; Park, S. Y. *J. Phys. Chem. C* **2007**, 111, 4052–4060.
- (14) Chao, K.; Shao, K.; Peng, T.; Zhu, D.; Wang, Y.; Liu, Y.; Su, Z.; Bryce, M. R. *J. Mater. Chem. C* **2013**, 1, 6800–6806.
- (15) (a) Marchi, E.; Sinisi, R.; Bergamini, G.; Tragni, M.; Monari, M.; Bandini, M.; Ceroni, P. *Chem. - Eur. J.* **2012**, 18, 8765–8773. (b) You, Y.; Seo, J.; Kim, S. H.; Kim, K. S.; Ahn, T. K.; Kim, D.; Park, S. Y. *Inorg. Chem.* **2008**, 47, 1476–1487.
- (16) Kim, J. B.; Han, S. H.; Yang, K.; Kwon, S. K.; Kim, J. J.; Kim, Y. H. *Chem. Commun.* **2015**, 51, 58–61.
- (17) Fan, C.; Li, Y.; Yang, C.; Wu, H.; Qin, J.; Cao, Y. *Chem. Mater.* **2012**, 24, 4581–4587.
- (18) Benjamin, H.; Zheng, Y.; Batsanov, A. S.; Fox, M. A.; Al-Attar, H. A.; Monkman, A. P.; Bryce, M. R. *Inorg. Chem.* **2016**, 55, 8612–8627.
- (19) Hoveyda, H. R.; Karunaratne, V.; Rettig, S. J.; Orvig, C. *Inorg. Chem.* **1992**, 31, 5408–5416.
- (20) Brain, C. T.; Paul, J. M. *Synlett* **1999**, 1642–1644.
- (21) Nonoyama, M. *Bull. Chem. Soc. Jpn.* **1974**, 47, 767–768.
- (22) Baranoff, E.; Curchod, B. F.; Frey, J.; Scopelliti, R.; Kessler, F.; Tavernelli, I.; Rothlisberger, U.; Gratzel, M.; Nazeeruddin, M. K. *Inorg. Chem.* **2012**, 51, 215–224.
- (23) Lamansky, S.; Djurovich, P.; Murphy, D.; Abdel-Razzaq, F.; Kwong, R.; Tsyba, I.; Bortz, M.; Mui, B.; Bau, R.; Thompson, M. E. *Inorg. Chem.* **2001**, 40, 1704–1711.
- (24) Hay, P. J. *J. Phys. Chem. A* **2002**, 106, 1634–1641.
- (25) Tsuboyama, A.; Iwawaki, H.; Furugori, M.; Mukaide, T.; Kamatani, J.; Igawa, S.; Moriyama, T.; Miura, S.; Takiguchi, T.; Okada, S.; Hoshino, M.; Ueno, K. *J. Am. Chem. Soc.* **2003**, 125, 12971–12979.
- (26) Langer, V.; Koos, M.; Gyepesova, D.; Sladkovicova, M.; Luston, J.; Kronek. *Acta Crystallogr., Sect. C: Cryst. Struct. Commun.* **2005**, 61, o602–o606.
- (27) Takizawa, S.; Shimada, K.; Sato, Y.; Murata, S. *Inorg. Chem.* **2014**, 53, 2983–2995. (b) Sun, Q.; Mosquera-Vazquez, S.; Lawson Daku, L. M.; Guenee, L.; Goodwin, H. A.; Vauthey, E.; Hauser, A. J. *Am. Chem. Soc.* **2013**, 135, 13660–13663.

- (28) Sheldrick, G. *Acta Crystallogr., Sect. A: Found. Crystallogr.* **2008**, *64*, 112–122.
- (29) Burla, M. C.; Caliandro, R.; Camalli, M.; Carrozzini, B.; Cascarano, G. L.; De Caro, L.; Giacovazzo, C.; Polidori, G.; Siliqi, D.; Spagna, R. *J. Appl. Crystallogr.* **2007**, *40*, 609–613.
- (30) Dolomanov, O. V.; Bourhis, L. J.; Gildea, R. J.; Howard, J. A. K.; Puschmann, H. *J. Appl. Crystallogr.* **2009**, *42*, 339–341.
- (31) Sheldrick, G. *Acta Crystallogr., Sect. C: Struct. Chem.* **2015**, *71*, 3–8.